AIAA JOURNAL
Vol. 41, No. 10, October 2003

Experimental Investigations of Hypersonic Flow over Highly Blunted Cones with Aerospikes

Viren Menezes,* S. Saravanan,† G. Jagadeesh,‡ and K. P. J. Reddy§
Indian Institute of Science, Bangalore 560 012, India

Effectiveness of aerospikes/aerodisk assemblies as retractable drag-reduction devices for large-angle blunt cones flying at hypersonic Mach numbers is investigated experimentally in hypersonic shock tunnel HST2 using a 120-deg apex-angle blunt cone. An internally mounted accelerometer balance system has been used for measuring the aerodynamic drag on the blunt cone with and without forward-facing aerospikes at various angles of attack. The measurements indicate around 55% reduction in drag for the blunt cone with flat-disk spike at zero degree angle of attack for a freestream Mach number of 5.75. Surface convective heat-transfer rate measurements have been carried out on the blunt cone with a flat-disk tipped spike of varying length in order to locate the shock reattachment point on the blunt-cone surface. The measured heat-transfer rates fluctuate by about ±20% in the separated flow region as well as near the reattachment point indicating the unsteady flowfield around the spiked blunt cone. The shock structure around the 120-deg apex-angle blunt cone with a 12-mm-long flat-tipped aerospike has also been visualized using the electric discharge technique. The visualized shock structure and the measured drag on the blunt cone with aerospikes agree well with the axisymmetric numerical simulations.

Nomenclature

a, b	=	locations of the accelerometers from center of gravity of the model
C_d	=	drag force coefficient
C_L	=	lift force coefficient
$C(t)$	=	axial force
D	=	model base diameter
g	=	acceleration due to gravity, 9.81 m/s^2
H_w	=	initial wall enthalpy
H_0	=	free stream total enthalpy
L	=	spike length
L/D	=	spike-length-to-model-base-diameter ratio
M_s	=	primary shock Mach number
M_∞	=	freestream Mach number
$N(t)$	=	normal force
P_0	=	freestream total pressure
P_∞	=	freestream static pressure
$q(t)$	=	heat flux at time t
q_∞	=	freestream dynamic pressure
R_b	=	model base radius
Re_∞	=	freestream unit Reynolds number
S	=	distance along the surface from model nose
S_b	=	blunt-cone base area
St	=	Stanton number
T_0	=	freestream total temperature
T_∞	=	freestream static temperature
t	=	time
V_∞	=	freestream velocity
w	=	body weight
α	=	angle of attack
ρ_∞	=	freestream static density
ξ_1, ξ_2, ξ_3	=	measured accelerations

Presented as Paper 2002-2709 at the AIAA 22nd Aerodynamic Measurement Technology and Ground Testing Conference, St. Louis, MO, 24–26 June 2002; received 13 August 2002; revision received 31 March 2003; accepted for publication 13 May 2003.

*Research Student, Department of Aerospace Engineering.
†Scientific Officer, Department of Aerospace Engineering.
‡Assistant Professor, Department of Aerospace Engineering. Member AIAA.
§Professor, Department of Aerospace Engineering.

Introduction

VEHICLES with high lift-to-drag ratio in the usual paradigm are not considered in the hypersonic flight corridors because the convective heating to relatively sharp edges produces unacceptably high heating loads. Hence, interplanetary space missions usually employ blunt bodies with low lift-to-drag ratios. However, such vehicles also require some lift and control features to respond to uncertainties in atmospheric density and to achieve requisite accelerations. Therefore, it is very important to reduce the wave drag during the ascent stage to reasonable levels in practical missions by expending minimum amount of energy. Various techniques such as concentrated energy deposition along the stagnation streamline, retractable aerospikes ahead of the blunt body, forward-facing jet in the stagnation zone of a blunt body, and also supersonic projectiles fired in the upstream direction from the stagnation zone are being evaluated by many research groups around the world for keeping the drag of the blunt body to acceptable levels during its atmospheric ascent.

Among all of these techniques, use of a retractable spike appears to be the simplest yet an effective means of reducing drag on large-angle blunt cones usually employed in aeroassisted space maneuvers. There have been many investigations in the past on the use of aerospikes as passive drag-reduction devices at hypersonic speeds. Some of the important research contributions are briefly discussed here. Crawford[1] found that both the drag and heat-transfer rates over spiked hemispherical cylinders reduced with the increase in spike length at Mach 6.8. Maull[2] characterized the unsteady shock oscillations around different spiked bodies at hypersonic Mach number by carrying out exhaustive experiments in the gun tunnel. Wood [3] extended Maull's investigation to spiked cone cylinders at Mach 10 and discovered five distinct types of flows concerning spiked bodies. Panaras[4] gave an insight into pulsating flows about axisymmetric spiked bodies, whereas Hutt and Howe[5] described the coupled flow effects of spiked bodies with different cross-section forebodies in supersonic flow. Kubota et al.,[6] Huebner et al.,[7] Sakagoshi et al.,[8] and Gnemmi et al.[9] have also studied the feasibility of using spikes as drag and heat-transfer rate reducing devices on blunt bodies at hypersonic speeds. Besides these investigations, flows around spiked bodies have been simulated numerically by several researchers.[10–12] Other than use of spikes, techniques such as deposition of energy in front of the body by focusing either laser or microwave beams.[13] directing gas jets from the nose of the body into the freestream,[14]

energy deposition using a plasma torch,[15] arc discharge,[16] and dc corona discharge[17] have also been considered for aerodynamic drag reduction.

Most of the reported investigations on spiked bodies have been carried out using slender blunt-nosed missile-shaped configurations, and more importantly the drag coefficient in these cases is deduced from the pressure measurements over the body surface. However to the best of our knowledge, the aerodynamic drag around generic spiked blunt bodies has not been measured directly at hypersonic Mach numbers. Such an experimental database is essential for validating numerical codes, which are used for optimizing the aerodynamic control features around large-angle blunt cones used in aeroassisted space missions. This investigation focuses on direct measurement of the drag force on a large-angle blunt cone fitted with different generic aerospikes at a nominal Mach number of 5.75. The drag force is measured using an internally mounted accelerometer force balance system in the Indian Institute of Science (IISc) hypersonic shock tunnel HST2 at a nominal stagnation enthalpy of 1.2 MJ/kg.

In the present investigations a 120-deg-apex-angle blunt cone has been used as the fore body in all of the experiments. Drag force measurements have been carried out using four types of aerospikes attached to the blunt cone in the stagnation point. Theoretically the flow separation resulting from a protruding aerospike can be judiciously utilized to achieve substantial drag reduction over blunt bodies. The macroscopic flow features around these four different aerospike configurations attached to the blunt cone are schematically shown in Fig. 1. The shock stand-off distance ahead of the blunt cone is enhanced by the flow separation induced by the aerospike, thereby minimizing the stagnant flow region, which in turn reduces the wave drag associated with the bow shock wave. From basic gas dynamics point of view, for maximum drag reduction the protruding length and geometry of the spike should be suitably selected so as to establish a large separation bubble on the face of the blunt cone, which will shift the flow reattachment zone off the shoulder of the body.

The main objectives of the present study are 1) visualization of the shock structure around spiked blunt cones using electric discharge technique, 2) design and fabrication of an internally mountable three-component accelerometer balance system for measuring the fundamental aerodynamic force coefficients for spiked blunt cones, 3) evaluation of various aerospike configurations as possible aerodynamic drag reduction devices for blunt-body configurations, 4) characterization of separation bubble on the blunt cone using the measured convective heat-transfer rates to the spiked blunt cone using platinum thin-film sensors, and 5) performance of illustrative numerical simulations using commercial computational-fluid-dynamics (CFD) code to complement the experiments. The details of this study are discussed in the subsequent sections.

Experiments

Facility

The HST2 hypersonic shock tunnel is schematically shown in Fig. 2. The shock-tube portion of HST2 consists of a 50-mm-inner-diam stainless-steel driver and driven sections separated by a metal diaphragm. Platinum thin-film sensors located toward the end of the driven section monitor the shock-wave velocity. The pressure jump across the shock wave is measured using a pressure transducer (PCB; Piezotronics) located at the end of the driven section. The wind-tunnel portion of the HST2 comprises a truncated conical nozzle terminating into a 30 × 30 cm size test section. The typical test conditions of the experiments with their repeatability margins are given in Table 1. The tunnel is capable of producing a reservoir enthalpy of up to 5 MJ/kg and has an effective test time of about 800 μs. Figure 3 shows a pressure history indicating the steady-state test time in the tunnel test section, along with an accelerometer recorded drag signal. A transient PC-based data-acquisition system with requisite software is used for recording and processing of the data from the tunnel.

Introducing an aerospike ahead of the blunt cone will induce pronounced unsteady shock oscillations in the flowfield at hypersonic

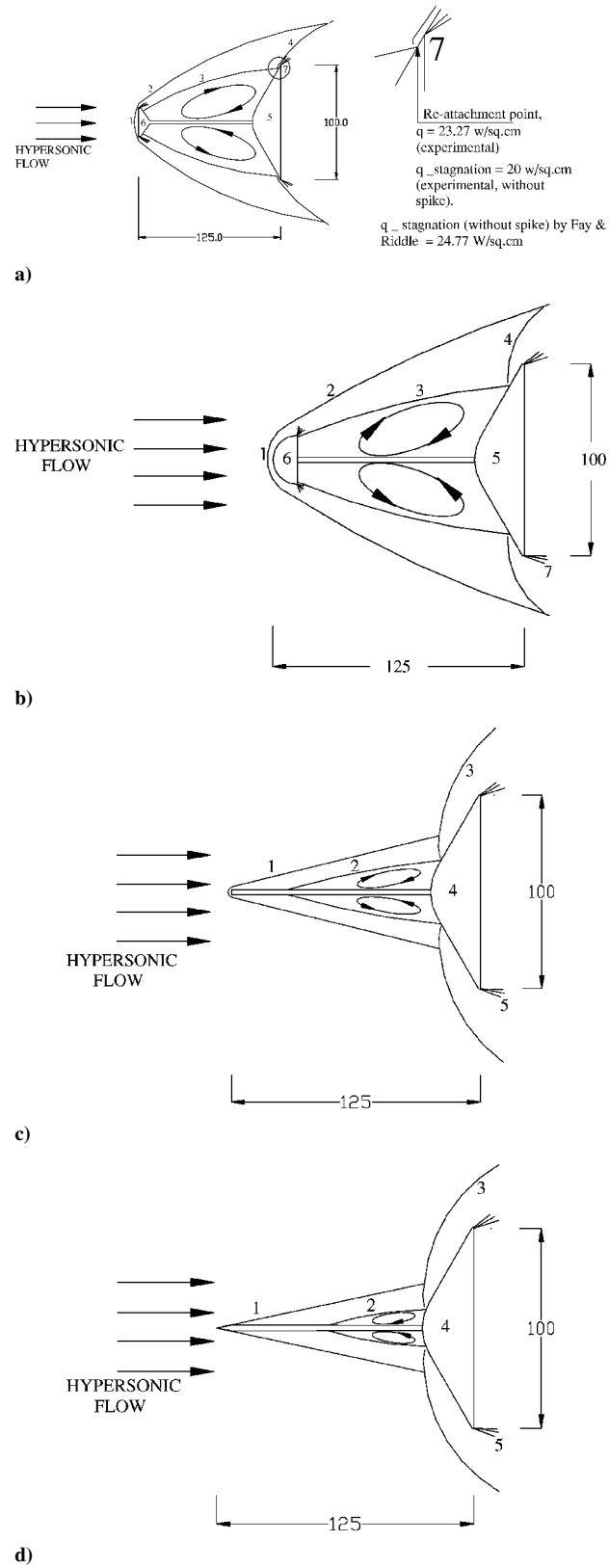

Fig. 1 Schematic representation of the flowfield features around the blunt cone with a) flat disk-tipped spike: 1, disk bow shock; 2, flow separation shock; 3, separation bubble; 4, reattachment shock; 5, blunt cone model; 6, aerodisk assembly; and 7, expansion fan; b) hemispherical disk-tipped spike: 1, disk bow shock; 2, flow separation shock; 3, separation bubble; 4, reattachment shock; 5, blunt cone model; 6, aerodisk assembly; and 7, expansion fan dimensions in millimeters; c) flat tipped spike: 1, spike oblique shock; 2, separation bubble; 3, reattachment shock; 4, blunt cone model; and 5, expansion fan and; d) sharp tipped spike: 1, spike oblique shock; 2, separation bubble; 3, reattachment shock; 4, blunt cone model; and 5, expansion fan.

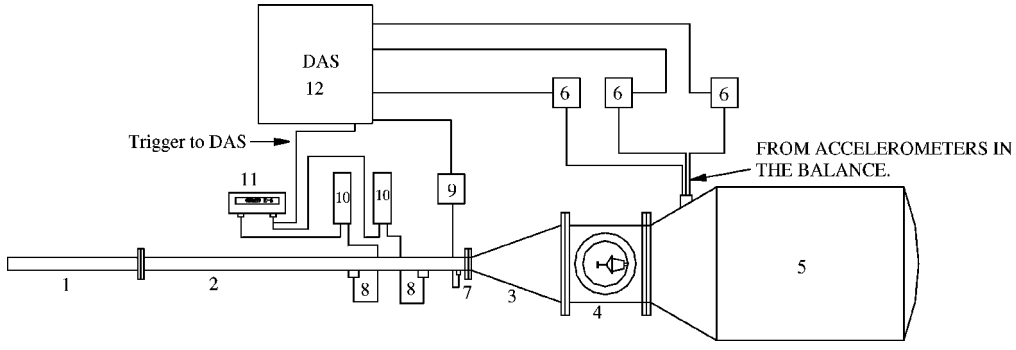

Fig. 2 Schematic diagram of the IISc hypersonic shock tunnel HST2: 1, driver section; 2, driven section; 3, Mach 5.75 conical nozzle; 4, test section; 5, dump tank; 6, accelerometer power supplies; 7, pressure transducer; 8, thermal sensor ports for shock speed; 9, pressure transducer power supply; 10, thermal sensor power supplies; 11, universal counter for shock speed; and 12, computer based data acquisition system.

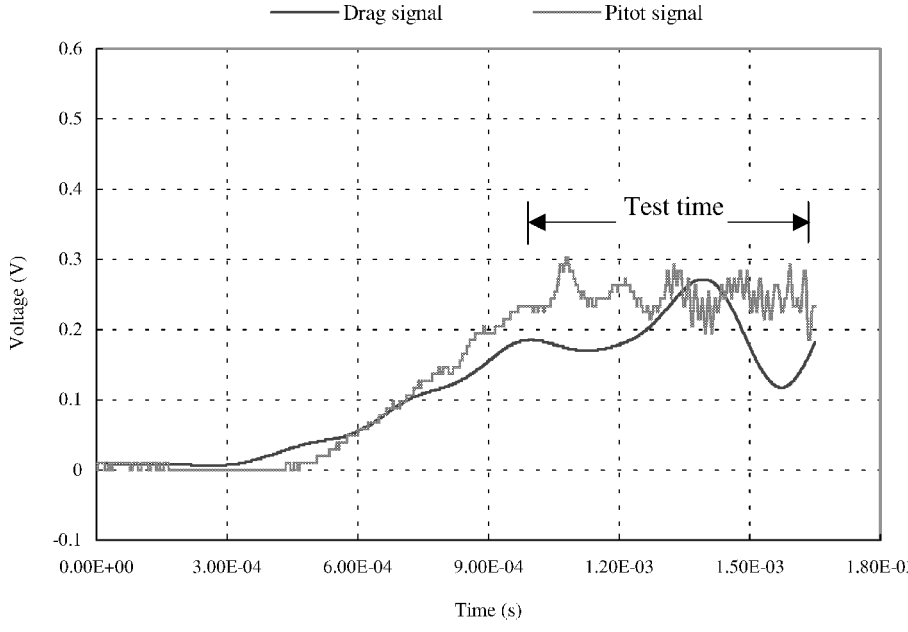

Fig. 3 Typical pitot signal (pressure history) obtained in the test section of HST 2 shock tunnel, indicating the steady flow time, superimposed on an accelerometer-measured drag signal for the model.

Table 1 Test conditions achieved in HST2 hypersonic shock tunnel

Tunnel parameter	Value
Driver gas	Helium
Test gas	Air @ STP
M_s	$3.1 \pm 5\%$
P_0, kPa	$500 \pm 6\%$
T_0, K	$1200 \pm 7\%$
H_0, MJ/kg	$1.206 \pm 7\%$
P_∞, kPa	$0.425 \pm 6\%$
T_∞, K	$140 \pm 7\%$
ρ_∞, kg/m^3	$0.01 \pm 9\%$
V_∞, m/s	$1400 \pm 4\%$
Re_∞, /m	$1.5 \times 10^6 \pm 1\%$

Mach numbers. Before one tries to make quantitative measurements on spiked blunt cones, it is essential to ensure that the shock structure from the spike does not interact with the test-section boundary layer. Hence, in the present study the shock structure around the spiked blunt cone is visualized before the drag measurements.

Flow-Visualization Experiments

The flowfield around the large-angle blunt cone with aerospike is visualized using electrical discharge technique.[18] The 70-mm-base-diameter blunt-cone model used in this experiment is fabricated using Bakelite hylem and fitted with a 2 (ϕ) $\times$ 12 mm (long) flat-headed steel aerospike. An electric discharge of about 2-μs duration is created, after attaining the steady flow conditions in the test section, between a point electrode suspended from the roof of the test section and a line electrode flush mounted on the spiked blunt cone. The spontaneous light emitted by the molecules in the discharge path in the hypersonic flow is photographed through the test-section window using either a digital camera or an ordinary camera loaded with ASA 1600 film in the bulb exposure mode. The visualized flowfields around the blunt cone with and without the aerospike are shown in Figs. 4a and 4b, respectively. These photographs show a clear flow separation shock originating at the tip of the spike and impinging on the model shoulder where the flow gets reattached. The experimentally measured flow separation shock angle of 43 deg matches well with the numerically computed value of 45 deg. Although not reported here, exhaustive flow-visualization experiments have been carried out on the blunt cone fitted with various spike geometries in order to understand the flowfield features around spiked blunt cones. These studies are carried out at the initial stage so as to optimize both the size and geometry of the spike as well as to design the model configurations for drag-reduction experiments in the shock tunnel. The results shown in Fig. 4 are a part of the experiment carried out to validate the commercial code CFX-TASCflow that has been used for numerical simulations in this

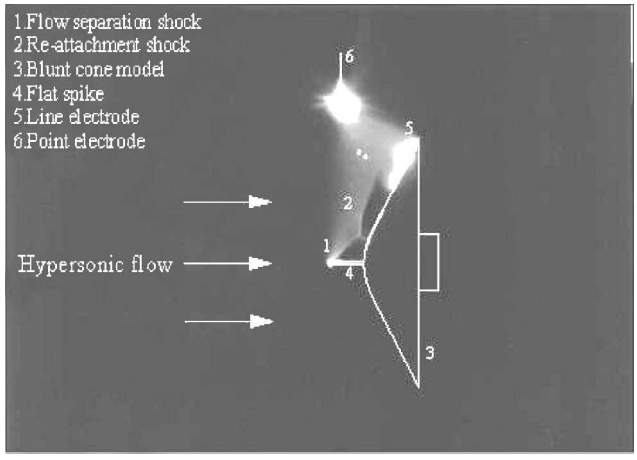

a)

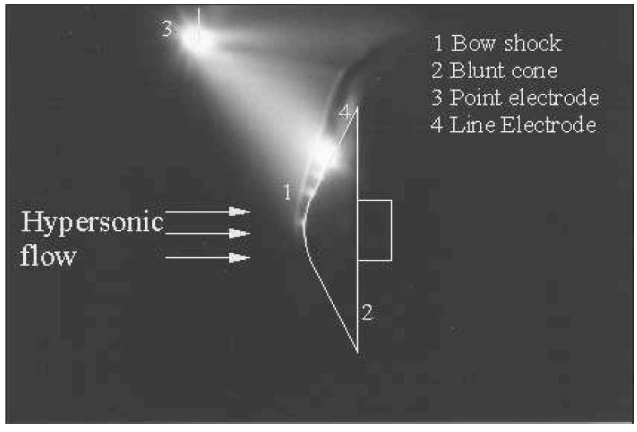

b)

Fig. 4 Flowfields around a) the spiked blunt cone and b) the blunt cone without spike, visualized using electrical discharge technique at Mach 5.75.

study. These results also ascertain the quality of the hypersonic flow in the tunnel test section and demonstrate the applicability of this flow-visualization technique to spiked-body flowfields.

Drag Measurements on Spiked Blunt Cones

The 120-deg blunt cone with a detachable forward-facing flat aerodisk-tipped spike along with other types of spikes used in this study is shown schematically in Fig. 5. The ratio of spike length to model base diameter is fixed at one in all model configurations in the present study. The drag force on the model is measured using a three-component accelerometer balance system,[19] shown in Fig. 5. The balance with two stainless-steel rings of 50-mm external diameter is mounted in the hollow region bored in the model skirt. The two metallic rings get fastened to the wall of the model skirt by means of threaded screws. Each ring is internally fixed with a flexible rubber bush that has a central hole. These bushes are adhesively bonded through their external surfaces to the internal surfaces of the metallic rings. A sting is glued to these bushes through their central holes, which supports the model with the balance in the test section. These two rubber bushes act as lift springs while in compression or tension and both act as drag springs in shear, thus forming a flexible suspension system in conjunction with the central fastening sting. The front lift and aft-lift accelerometers are mounted onto the metallic arms of the balance that stretch out from the rings. The drag accelerometer is screwed onto the inner surface of the blunt cone along the axis of the model as shown in Fig. 5.

The rear skirt of the model is used only as a housing for the balance, and there exists a step between the 120-deg blunt-cone base and the skirt, which brings about a flow separation behind the cone and all over the skirt surface. During the short run times encountered in the shock tunnel, the model along with the accelerometers moves as a free body, and the resulting accelerations in the axial and vertical directions are measured from the outputs of the corresponding accelerometers. The PCB-piezotronics accelerometers, with sensitivity and frequency range of 10 mV/g and 10 kHz, respectively, have been used in the balance system. The axial force $C(t)$ and normal force $N(t)$ on the model are calculated from the following equations[19]:

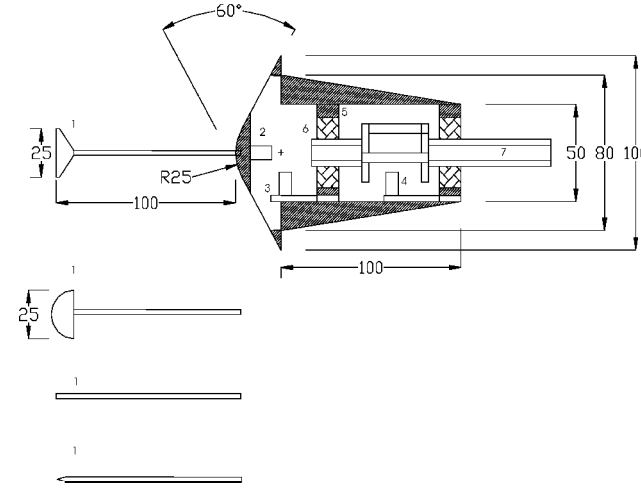

Fig. 5 Schematic diagram of the 120-deg-apex-angle blunt cone fitted with a three-component accelerometer balance system along with different types of aerospikes: 1, aerospike assembly; 2, drag accelerometer; 3, front lift accelerometer; 4, aft. lift accelerometer; 5, steel housing for the bush; 6, rubber bush; and 7, fastening sting all dimensions in mm.

$$C(t) = [w/g]\xi_3 \tag{1}$$

$$N(t) = [(w/g)/(a+b)](b\xi_1 + a\xi_2) \tag{2}$$

The aerodynamic drag coefficient C_d and lift coefficient C_L are computed from these values using the relations

$$C_d = [C(t)/(q_\infty S_b)]\cos\alpha + [N(t)/(q_\infty S_b)]\sin\alpha \tag{3}$$

$$C_d = [N(t)/(q_\infty S_b)]\cos\alpha - [C(t)/(q_\infty S_b)]\sin\alpha \tag{4}$$

The measured drag coefficient for the blunt-cone model with and without forward-facing aerospikes at various angles of attack is shown in Fig. 6. Figure 7 indicates the variation of percentage of drag reduction with respect to angle of attack for the model with different spikes. From these results it is clear that at lower angles of attack (up to ~5 deg), about 40–55% drag reduction is measured with flat and hemispherical faced aerodiscs. These two spike geometries keep most of the area on the cone surface under their aerodynamic shadow,[20] thereby creating a large flow separation bubble in that area and hence push the flow reattachment zone/shock towards the tip of the cone shoulder at lower angles of attack. The flow separation bubble is a region of low pressure and temperature. The flat-faced aerospike without any disk results in ~20% drag reduction at 0-deg angle of incidence while with the sharp-tipped aerospike an increase in aerodynamic drag at all angles of attack other than 0 deg is observed because these spike geometries are unable to provide any aerodynamic shadow to the model forebody, and hence the flow reattachment zone in these two cases shifts very close to the nose of the model creating larger surface pressures. As the angle of attack is increased to 10 deg, the drag on the spiked body exceeds that of the body without spike in all the cases as a result of the inward shift of the flow reattachment point on the forebody of the blunt cone on the windward side. Though the model used in this case is nonlifting in nature, it generates sufficient aft lift at higher angles of attack when the spike is attached to its nose, a characteristic that might be helpful during aeroassisted orbit transfer. This observation substantiates the reattachment phenomenon just explained.

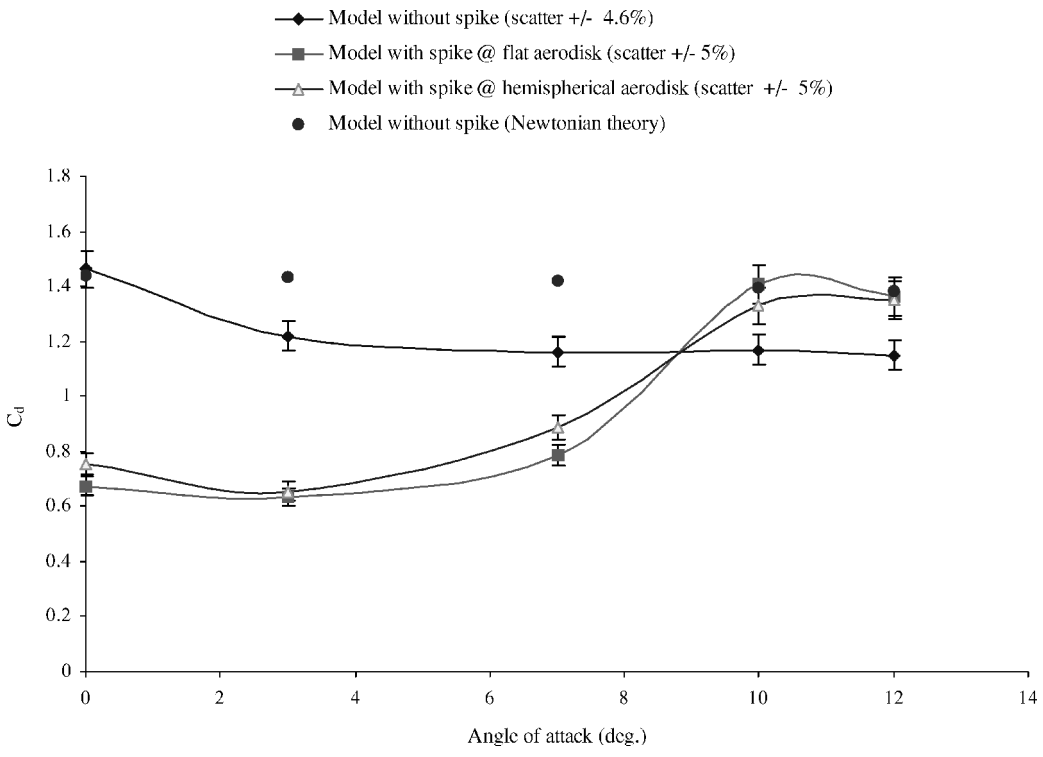

a)

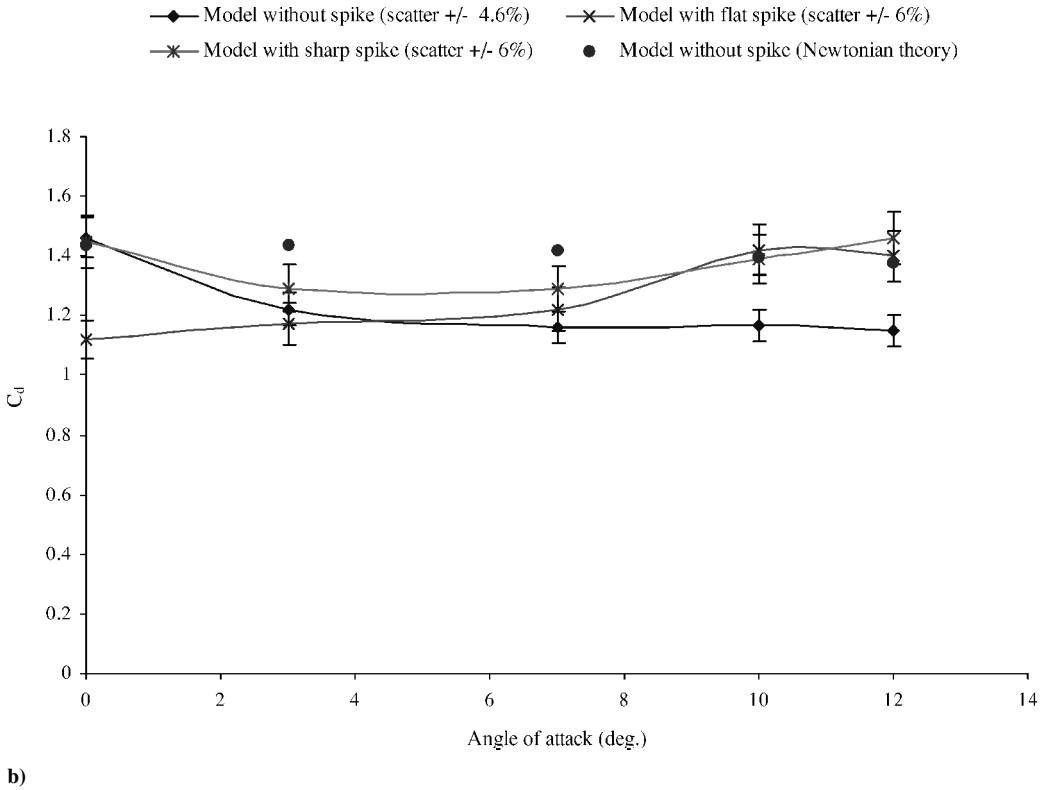

b)

Fig. 6 Variation of drag coefficient with angle of attack for 120-deg blunt-nosed cone with and without a) disk-tipped spikes and b) disk-less spikes.

The drag curve for the body without spike droops downward as the angle of attack increases, and this can be attributed to the fact that the larger surface area of the blunt cone on the leeward side is being engulfed by the expanding flow at higher angles of attack. Theoretical values of drag coefficient for the blunt cone (rear skirt not considered) without spike estimated using Newtonian theory[21] are also shown in Fig. 6. It is seen that the trend of variation of the theoretical estimations with increasing angle of attack is identical to the experimental values.

One of the important observations from the results presented in Figs. 6 and 7 is that the aerospike with flat aerodisk reduces the drag on the blunt cone substantially compared to all of the other configurations.[22] We have investigated the effect of the length of the aerospike on the drag reduction for this configuration. These results are presented in Fig. 8, which show the variation of C_d with the length of the spike fitted with the flat aerodisk. As the length of the spike is reduced, the angle of inclination of the separation zone increases, which in turn would increase the angle of the flow

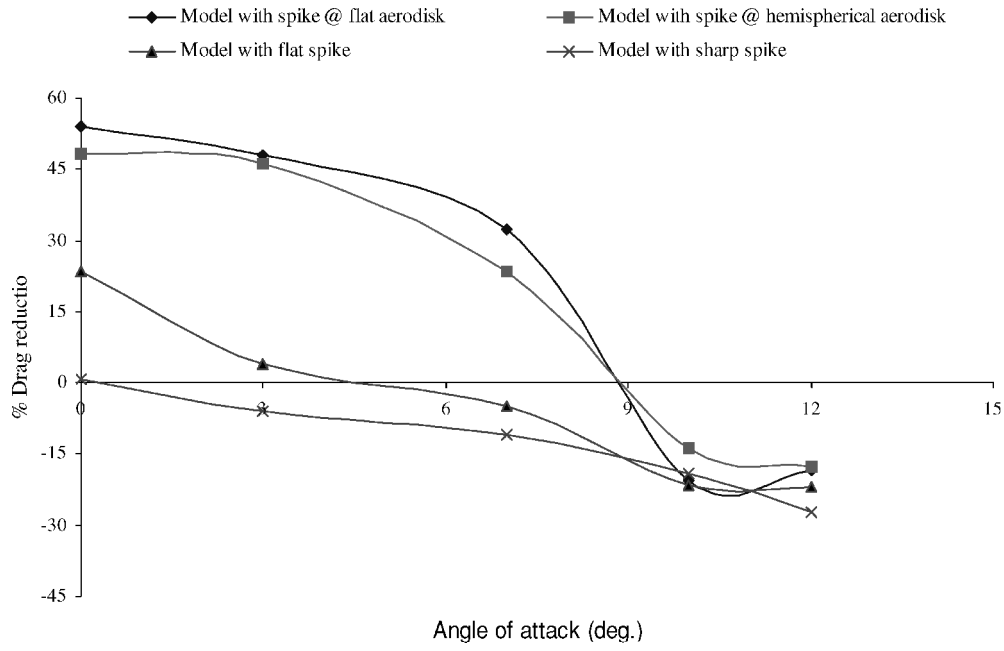

Fig. 7 Variation of percentage of reduced drag with angle of attack for the spiked 120-deg blunt cone at Mach 5.75.

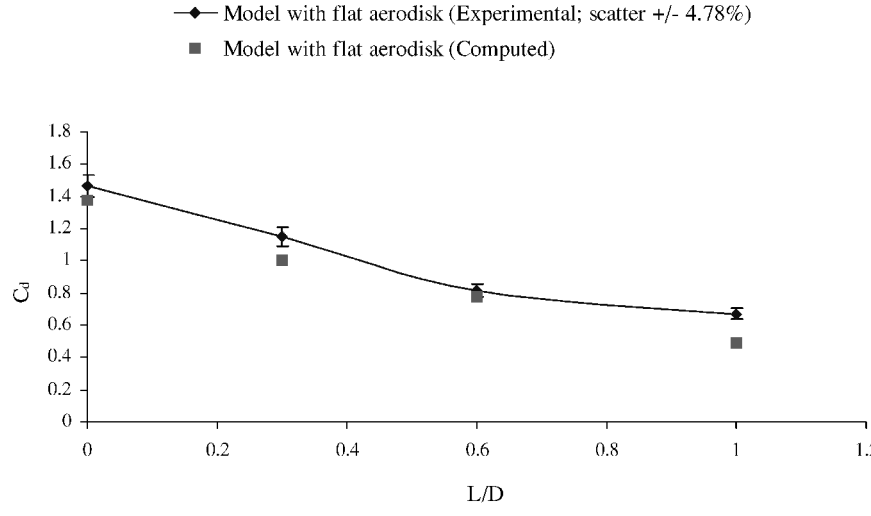

Fig. 8 Variation of drag coefficient for the 120-deg blunt cone with flat aerodisk-tipped spike at different L/D.

separation shock,[23] increasing the pressure and density behind the shock within the separation bubble. Hence the drag on the forebody increases with the decrease in spike length.

The geometry and the size of the aerospike for maximum drag reduction should be such that the flow reattachment point is moved off of the vehicle forebody and the entire front face of the vehicle is submerged in the separated flow. To precisely locate the reattachment point on the blunt-cone surface, convective heat-transfer measurements are carried out using platinum thin-film sensors.

Heat-Transfer Measurements

For understanding the fluid-dynamic implications of adding a spike to the blunt body, it is important to quantify accurately the separation bubble on the blunt cone. The decrease and increase of the surface heat-transfer rates during separation and reattachment, respectively, will be an accurate measure of the size of the separation bubble on the blunt cone. Platinum thin-film sensors deposited on the ceramic glass (Macor) inserts, which are embedded in the metallic blunt-cone model, are used to measure the surface convective heat-transfer rates. Thin film sensors are deposited on the Macor using platinum 05-X metallo-organic ink (M/s Englehard-Clal, United Kingdom). The sensors are powered through constant current (~20 mA) sources and connected to the PC-based data-acquisition system. The initial resistance of these passive gauges is maintained at around 50 Ω. The change in the voltage across the gauge with respect to time gives the temperature time history at the gauge location on the model surface. These temperature time-history signals are then numerically integrated[24] in order to get the convective surface heat-transfer rates. The details of the instrumentation used in heat-transfer measurements along with the detailed data-reduction methodology have been discussed in Ref. 24.

Figure 9 gives the variation of Stanton number with respect to the nondimensional gauge locations (S/R_b) on the model surface at 0-deg angle of attack. The surface heat-transfer rates have been nondimensionalized in the form of Stanton number based on the tunnel freestream conditions, given by the expression

$$St = \frac{q(t)}{[\rho_\infty V_\infty (H_0 - H_w)]} \tag{5}$$

The separation region on the body surface is indicated by low and fluctuating heat-transfer rates because of the low-temperature

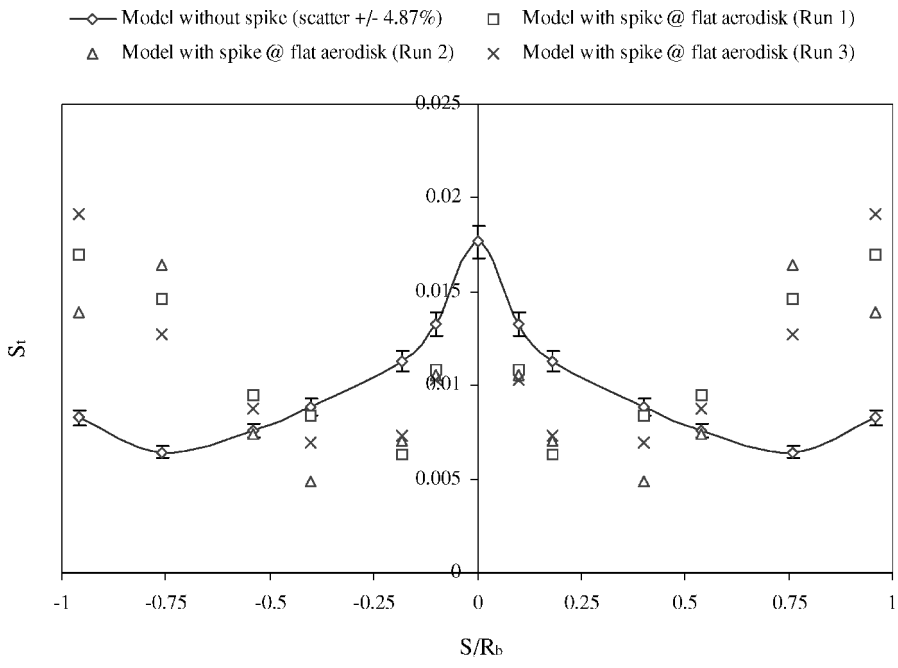

Fig. 9 Distribution of measured Stanton number along the surface of 120-deg blunt cone at 0-deg angle of incidence.

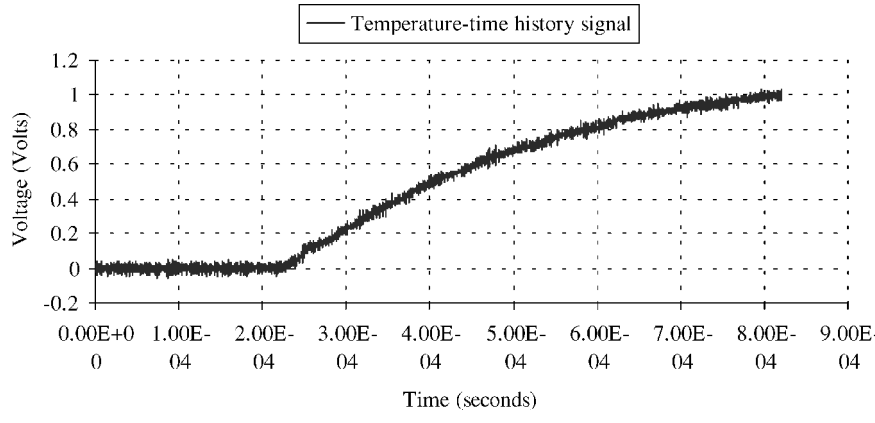

Fig. 10 Steady temperature–time history signal obtained from a platinum thin-film sensor mounted on the model without spike.

unsteady flow in that region.[25] The flow separates in the wake of the aerodisk on the spike as a result of the combined effects of friction offered by the spike/disk surface as well as the adverse pressure gradients created by the aerodisk shock wave and the body geometry. This separated flow, in the form of a large bubble comprising flow reversals on the spike and the blunt-body surface, is unsteady and oscillating in nature.

Figure 10 shows a typical temperature–time history recorded by a platinum thin-film sensor on the model without any spike. In this case the flow is attached and has attained steady state over the model surface, which is exhibited by the parabolic shape of the temperature–time history signal. Figure 11 shows a temperature–time history signal recorded by a platinum thin-film gauge in the flow separation zone on the spiked model. Unlike the previous case, the signal in Fig. 11 is not of a perfect parabolic shape, which is a clear indication of the flow being unsteady in that region. For all of the shots taken over the model without spike, the temperature–time history on the model surface has been of parabolic shape as shown in Fig. 10, and for the model with spikes the recorded temperature–time history has been unsteady as in Fig. 11.

For a given spike length and shoulder bluntness on a spiked body, if the flow just outside the separated shear layer approaching the body's shoulder can be turned by an attached conical shock, then the shock structure is stable because an equilibrium condition is reached between escaping and recirculating flows in the separated region, and no oscillations occur. If the turning angle of the flow is too large to be accomplished by an attached conical shock, a detached strong shock is generated, which pumps high-pressure flow from the reattachment region at the body's face into the recirculating region of the separated shear layer. This high-pressure flow that gets into the separated flow region inflates the separation bubble, and the shock structure is pushed upstream. This gives rise to self-excited shock oscillations during which the conical foreshock and the accompanying shear layer oscillate laterally and their shape changes periodically from concave to convex. This type of flowfield is unsteady in nature. The separated shear layer with an inflection point in the velocity profile is inherently unstable,[26] and when this hits the body at the reattachment point selective amplification of the disturbances takes place, and this would cause the surface heat-transfer rates to fluctuate at the point of reattachment. The point of reattachment could be shifting to and fro along the body surface because of these shock oscillations.

Because of this unsteady oscillation of the separation bubble, pronounced variations in the locations of separation shock, body shock ahead of the blunt cone, and the reattachment point on the blunt-cone surface are observed in different runs with identical freestream

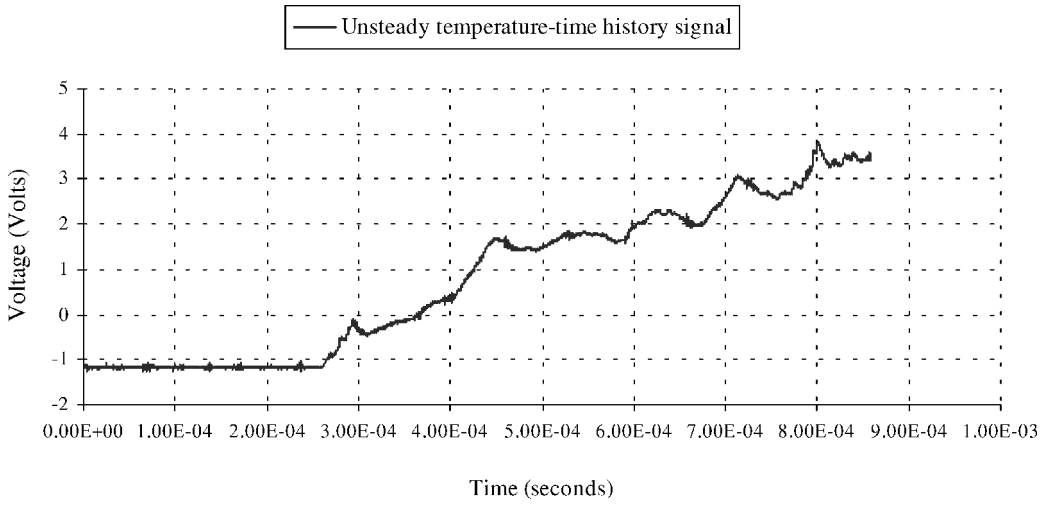

Fig. 11 Unsteady temperature–time trace of a thin-film gauge from a flow separation zone on the spiked blunt cone.

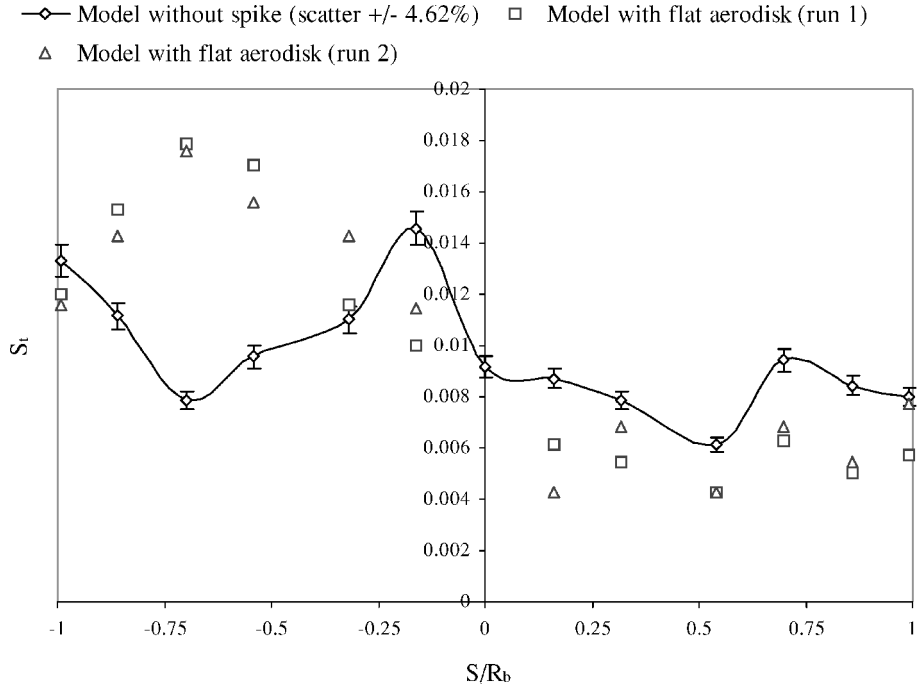

Fig. 12 Distribution of measured Stanton number along the surface of 120-deg blunt cone at 7-deg angle of incidence.

conditions. This is indicated by the scatter in the measured heat-transfer rates on the cone, especially in the separated region, as seen in Fig. 9. Also, the sudden jump in the measured heat-transfer rates towards the edge of the spiked cone is not very high when compared to the stagnation point heat-transfer rate on the blunt cone without spike. This indicates that the flow reattachment zone is somewhere very near the edge of the cone but is off of the body. This shows that the deployed aerospike assembly has been successful in pushing the flow reattachment point just off of the edge of the cone. Figures 12 and 13 give the Stanton-number distribution on the preceding spiked model surface at 7- and 12-deg angle of incidence, respectively. The inward shift in the point of flow reattachment on the windward side of the model can clearly be seen in these figures in the form of inward-shifting enhanced heat-transfer rates.

To investigate the effect of the model size on the unsteady oscillatory behavior of the spiked-body flowfield, further heat-transfer measurements are carried out on a blunt-cone model with flat-disk spike, reduced by 50% in size, retaining the geometrical similarity. The heat-transfer measurements are also carried out with varying spike length for the preceding spike geometry. The results of this experiment are shown in Fig. 14. The measured heat-transfer rates in this case exhibit less scatter near the nose of the model indicating reduced flow unsteadiness in that region and also the signal quality has been improved (in comparison with the larger size model) because of an increased flow density within the separation bubble. But the scatter persists at or in the vicinity of flow reattachment point at the outer edge.[25] More scatter in the data has been observed at the model outer edge for reduced spike lengths. However, with decrease in spike length the flow reattachment zone on the model surface does not exhibit any major shift in its position, as indicated by the enhanced heat-transfer rates at the last gauge location towards the edge of the model, as shown in Fig. 14. So even at a L/D of 0.2, this particular spike geometry is capable of keeping almost the complete blunt body in the aerodynamic shadow region, causing substantial surface heat-transfer rate reduction near the nose portion. The numerically simulated flowfield pictures in Fig. 15 give an insight into the preceding statement.

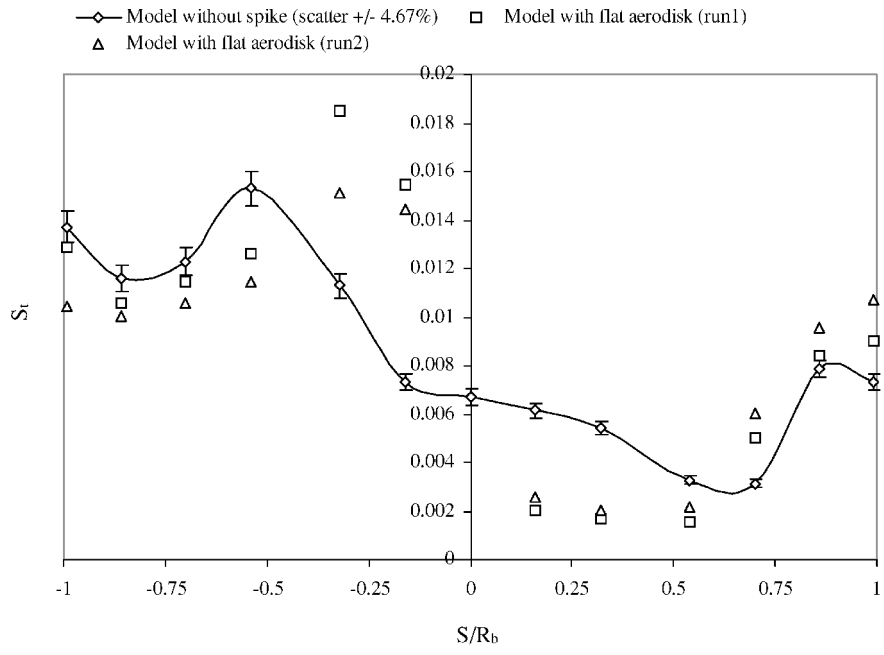

Fig. 13 Distribution of measured Stanton number along the surface of 120-deg blunt cone at 12-deg angle of incidence.

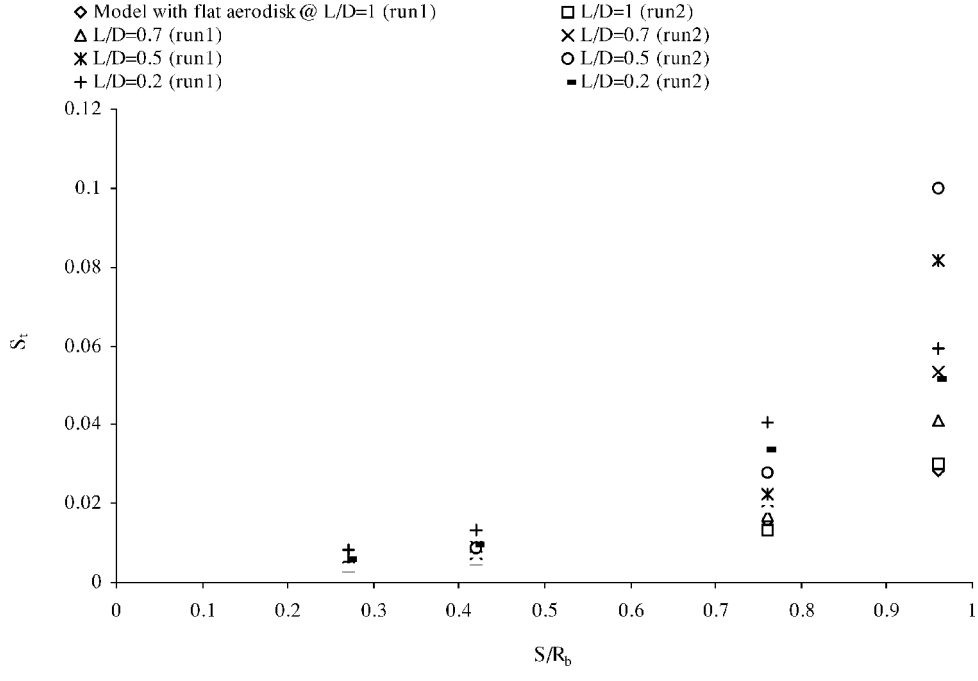

Fig. 14 Distribution of measured Stanton number along the surface of 120-deg blunt cone (scaled-down) model with flat disk-tipped spike at different *L/D*, at 0-deg angle of incidence.

Measurement Uncertainties

The estimated uncertainties in the measured data are $\Delta C_d = \pm 0.09 C_d$, $\Delta q_\infty = \pm 0.072 q_\infty$, and $\Delta St = \pm 0.108 S_t$. The uncertainty analysis is carried out based on Ref. 27. Uncertainties in the sensor sensitivities, setting of angle of attack, output of the data-acquisition systems, and the restraint offered by the rubber bushes to the free flight of the model during test time are some of the factors that contribute to the uncertainties in C_d. The uncertainties in the tunnel freestream pressure and freestream Mach number give rise to the uncertainty in q_∞ just mentioned. Based on the uncertainties associated with the gauge characteristics, data-acquisition system, data-reduction techniques and calibration, the measured values of heat-transfer rates are believed to be accurate to ±5% with helium as driver gas. Various factors such as uncertainty in angle of attack, misalignment of Macor inserts, discontinuity in substrate and model properties, and departure from one-dimensional heat conduction during the run time contribute to the uncertainties in the measured Stanton number.

Numerical Study

To complement the experiments, illustrative numerical simulations are carried out using commercial CFD code CFX TASCflow.[28] Steady-state flowfields around the large-angle spiked blunt cone at 0-deg angle of attack are simulated using the two-dimensional axisymmetric compressible laminar CFX-TASCflow code. The code is a complete Navier–Stokes (N-S) solver that is capable of handling both incompressible and compressible flow problems for steady as

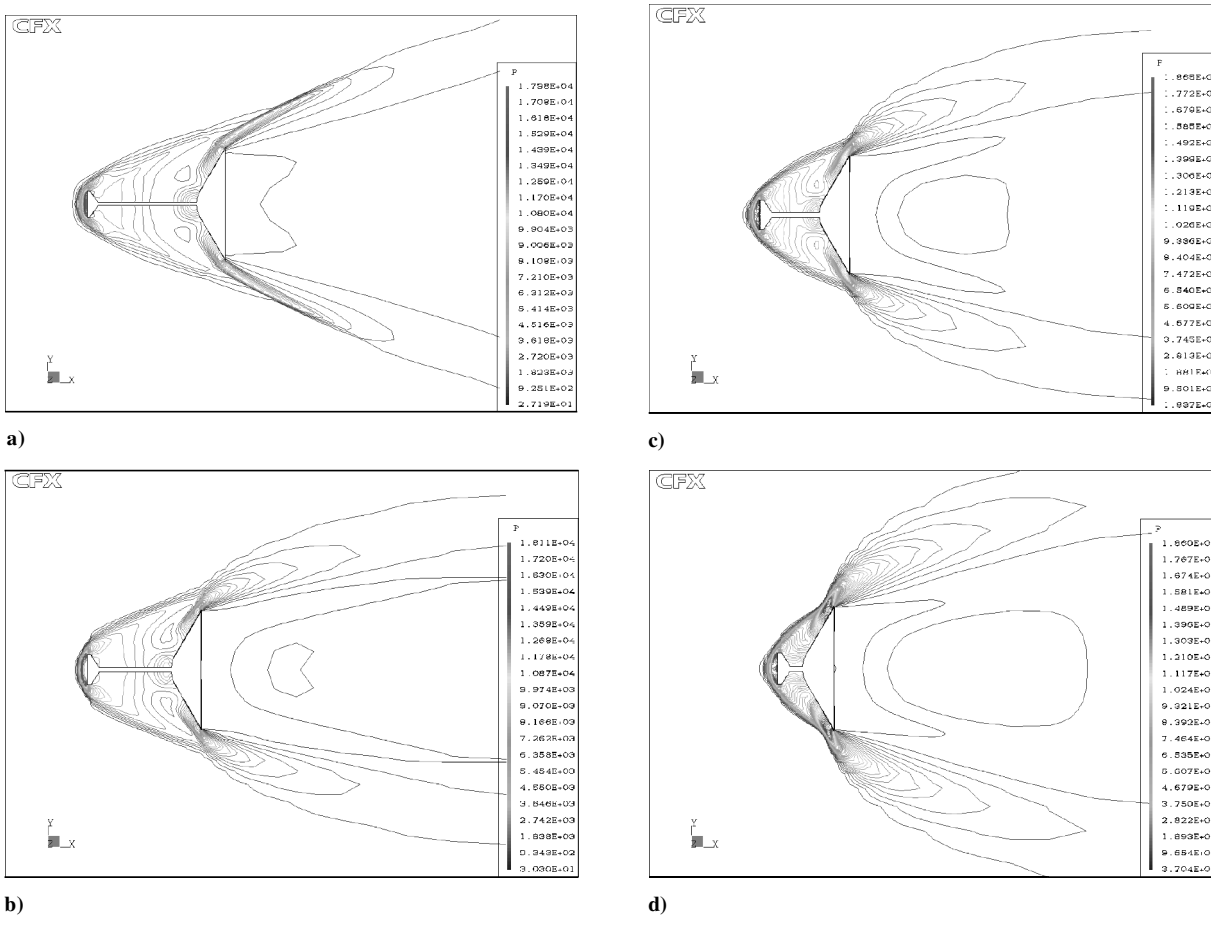

Fig. 15 Simulated flowfields around the 120-deg blunt cone fitted with a flat aerodisk at an *L/D* of a) 1, b) 0.7, c) 0.5, and d) 0.2.

well as unsteady flow domains. It has good grid-generating capabilities like nonorthogonal, curvilinear, and multiblock grids with embedded grid-refinement utilities. The discretization technique in this code consists of pressure-based formulation with conservative finite element based finite control volume method. The upwind-differencing discretization scheme has been used in the present study with a physical advection correction to increase the accuracy of the computation.

The boundary conditions used in this simulation are based on the experimental freestream conditions in the shock-tunnel test section, which are as follows:

1) *Inlet:* At this boundary of the computational domain, the velocity, static pressure, and static temperature of the flow have been specified. Typical values used in here are velocity $V = 1400$ m/s, pressure $P = 425$ Pa, and temperature $T = 140$ K. These are the flow properties obtained in the test section (freestream) of the shock tunnel for an enthalpy level of 1.2 MJ/kg.

2) *Outlet:* At the outlet of the computational domain, all variables are extrapolated from the interior domain, that is, a supersonic outlet is used at the nodes of the outlet region.

3) *Wall:* The wall boundary condition is used at the blunt-cone model surfaces, and the fluid at these surfaces is assumed to have a no-slip condition. A constant temperature of 300 K is specified at the walls.

4) *Symmetry:* Other bounds of the computational domain, excluding inlet and outlet, are specified as symmetry planes. The fluid velocity is assumed to be tangential at these symmetry planes.

A typical grid used for the computations of flowfields around the spiked blunt cone is shown in Fig. 16. The multiblock, structured grid used for the computations has a total number of around 25,836 nodes (grid points). The computation domain is reduced to one-half of the complete domain because of the symmetry of the problem. The grid cell height near the wall is around 8×10^{-5} m,

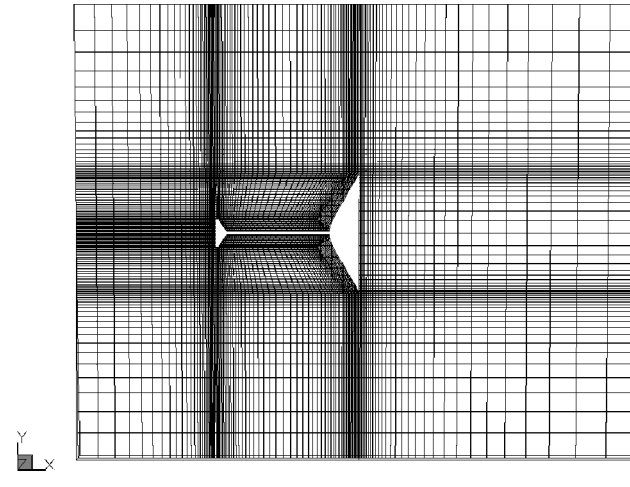

Fig. 16 Typical grid used in numerical computations for the large-angle spiked blunt cone.

and the computation is focused only on the model forebody. An upwind-differencing scheme has been used for the computations with a local time step of 0.9. The target residuals to terminate the simulation have been set at 1.0×10^{-4}, which allow obtaining a stationary converged solution of the problem. About 1500 iterations (time steps) have been used for the convergence. Approximately 3 h of CPU time were required for the simulation on an Intel Pentium 4, 1.4-GHz processor. The program was run on a Windows NT platform.

Table 2 shows both the experimental and the numerically computed values of drag coefficients for the blunt cone with and without

Table 2 Experimental and computed values of drag coefficient C_d at 0-deg angle of attack for 120-deg blunt cone model at a *L/D* of 1

C_d	Blunt cone	Blunt cone with flat aerodisk-tipped spike	Blunt cone with hemispherical aerodisk-tipped spike	Blunt cone with flat-faced spike	Blunt cone with sharp tipped spike
Experimental	1.462	0.6734	0.757	1.12	1.45
Numerical	1.374	0.49	0.74	0.95	1.14

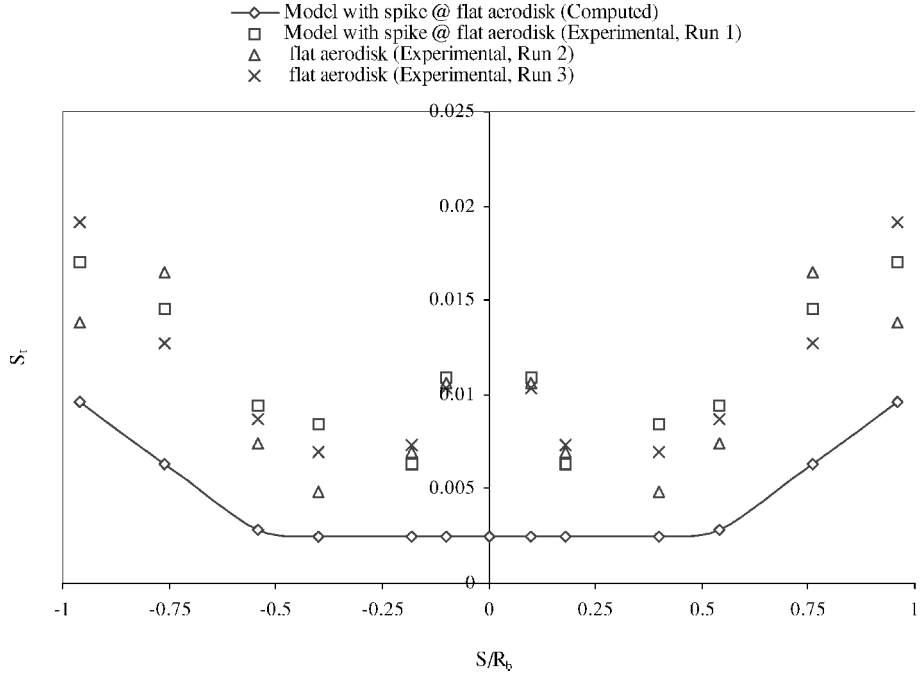

Fig. 17 Experimental and computed Stanton-number distribution for 120-deg blunt cone model with flat aerodisk at 0-deg angle of incidence.

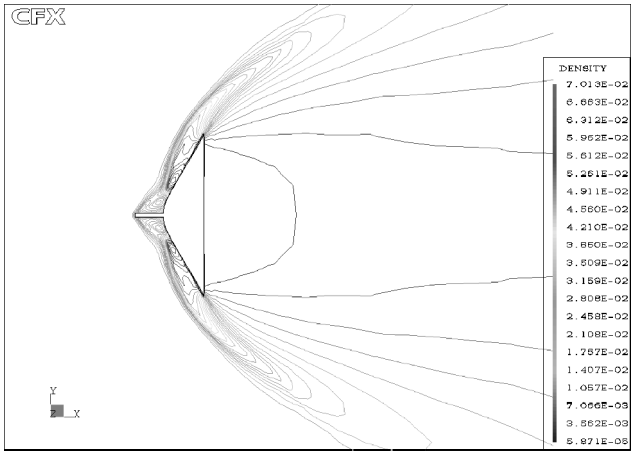

Fig. 18 Computed density field around the 120-deg blunt cone with 12-mm-long flat aerospike at Mach 5.75.

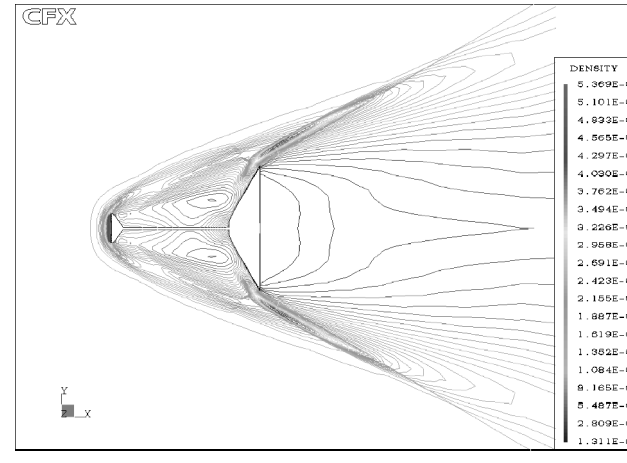

Fig. 19 Computed density field around the 120-deg blunt cone with flat aerodisk at Mach 5.75.

various spike geometries at 0-deg angle of attack and for a L/D of 1. Figure 17 shows the distribution of experimental and computed heat-transfer rates over the blunt cone surface with a flat aerodisk spike. Considerable differences can be seen between the experimental and the computed values of heat-transfer rates for the spiked body. The unsteady oscillations of separation bubble and the assumption of laminar flow boundary conditions are some of the important factors for the observed differences between experiments and the simulations.

The numerically simulated density field around the blunt cone with 12-mm-long, flat-faced aerospike is shown in Fig. 18. The simulated shock structure around the spiked body matches well with the visualization results shown in Fig. 4a. The simulated density distribution around the blunt cone with a flat aerodisk tipped spike is shown in Fig. 19. The reattachment point shifts toward the edge of the blunt cone for aerodisk-tipped spike, as seen in Fig. 19. This is also confirmed by the sudden jump observed in the measured heat-transfer rates near the edge of the blunt cone. The separation zone and the flow reattachment point can more clearly be seen in Fig. 20, which gives the computed Mach contours around the blunt cone with the flat aerodisk-tipped spike.

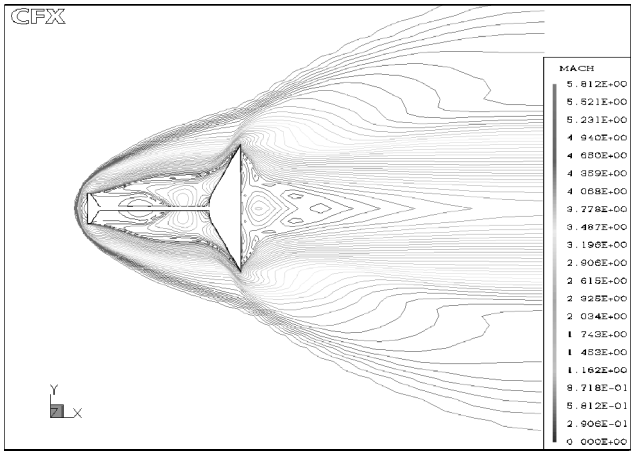

Fig. 20 Computed Mach contours around the 120-deg blunt cone with flat aerodisk.

Conclusions

The experimental results highlight the effectiveness of different types of forward-facing aerospikes as drag-reducing devices on large-angle blunt cones flying at hypersonic Mach number. For the 120-deg-apex-angle blunt cone with forward-facing disk-tipped aerospikes, a drag reduction of ~40–55% has been measured for small angles of attack at a nominal Mach number of 5.75. Spikes without aerodisks do not result in noticeable reduction in drag. At higher angles of attack, the drag on all spiked bodies increases as a result of the inward shift in the point of flow reattachment on the windward side of the cone. The drag on the body increases with decrease in the spike length because of an increase in the pressure within the separation bubble. Heat-transfer measurements on the body with a flat disk-tipped aerospike at 0-deg angle of attack show that the separation bubble completely engulfs the blunt cone in the aerodynamic shadow. This is clear from the substantially lower (~10 W/cm^2) values of heat-transfer rates measured on the blunt cone in that region. The flow reattachment zone is characterized by the sudden jump in the measured heat-transfer rates toward the outer edge of the cone. The fluctuations in the measured heat-transfer rates indicate the oscillatory behavior of the separation bubble. Heat-transfer measurements at 7- and 12-deg angles of attack show a clear inward shift in the point of flow reattachment on the windward side of the model in terms of measured enhanced surface heat-transfer rates. Measured surface heat-transfer rates with varying spike length indicate that most of the vehicle forebody could be kept under the aerodynamic shadow of the spike while retracting the spike. The surface heat-transfer rate measurements on scaled-down spiked model indicate a reduction in the magnitude of flow unsteadiness within the separation bubble near the nose of the model. Further experiments are underway to resolve the effect of dissociated flow on the effectiveness of aerospikes as drag-reduction devices at hypervelocity flows and also to study the hypersonic buzz phenomenon on the spiked blunt cones.

References

[1]Crawford, D. H., "Investigation of the Flow over a Spiked-Nose Hemisphere-Cylinder," NASA TN-D-118, Dec. 1959.

[2]Maull, D. J., "Hypersonic Flow over Axially Symmetric Spiked Bodies," *Journal of Fluid Mechanics*, Vol. 8, Pt. 4, 1960, pp. 584–592.

[3]Wood, C. J., "Hypersonic Flow over Spiked Cones," *Journal of Fluid Mechanics*, Vol. 12, Pt. 4, 1961, pp. 614–624.

[4]Panaras, A. G., "Pulsating Flows about Axisymmetric Concave Bodies," *AIAA Journal*, Vol. 19, No. 6, 1981, pp. 804–806.

[5]Hutt, G. R., and Howe, A. J., "Forward Facing Spike Effects on Bodies of Different Cross Section in Supersonic Flow," *Aeronautical Journal*, Vol. 93, No. 926, 1989, pp. 229–234.

[6]Kubota, H., Watanuki, T., Matsumoto, S., Fukui, T., and Suenaga, H., "Experimental Study on Flow over Spiked Hemisphere at Komaba Hypersonic Wind Tunnel," *Journal of the Faculty of Engineering, Tokyo University(B),* Vol. 42, No. 1, 1993, pp. 65–71.

[7]Huebner, L. D., Mitchell, A. M., and Boudreaux, E. J., "Experimental Results on the Feasibility of an Aerospike for Hypersonic Missiles," AIAA Paper 95-0737, Jan. 1995.

[8]Sakagoshi, A., Mihara, K., Watanuki, T., and Kubota, H., "Effectiveness of an Aerospike for Reduction of Hypersonic Aerodynamic Heating," *Procedings of 22nd International Symposium on Space Technology and Science*, ISTS 2000-e-23, Morioka, Japan, 2000.

[9]Gnemmi, P., Srulijes, J., Roussel, K., and Runne, K., "Flow Field Around Spike-Tipped Bodies," AIAA Paper 2001-2464, June 2001.

[10]Yamauchi, M., Fujii, K., and Higashino, F., "Numerical Investigation of Supersonic Flows Around a Spiked Blunt Body," *Journal of Spacecraft and Rockets*, Vol. 32, No. 1, 1995, pp. 32–42.

[11]Fujita, M., and Kubota, H., "Numerical Simulation of Flow Field over a Spiked Blunt-Nose," *Computational Fluid Dynamics Journal*, Vol. 1, No. 2, 1992, pp. 187–195.

[12]Kubota, H., Watanuki, T., Matsumoto, S., Fujita, M., and Fukui, T., "Effect of Spike Attached on a Hemisphere in Hypersonic Flow," *Proceedings of 19th International Symposium on Space Technology and Science*, Yokohama, Japan, 1994, pp. 363–369.

[13]Riggins, D., Nelson, H. F., and Johnson, E., "Blunt Body Wave Drag Reduction Using Focused Energy Deposition," *AIAA Journal*, Vol. 37, No. 4, 1999, pp. 460–467.

[14]Meyer, B., Nelson, H. F., and Riggins, D. W., "Hypersonic Drag and Heat-Transfer Reduction Using a Forward-Facing Jet," *Journal of Aircraft*, Vol. 38, No. 4, 2001, pp. 680–686.

[15]Marsh, J. J., Myrabo, L. N., Messitt, D. G., and Nagamatsu, H. T., "Experimental Investigation of Hypersonic Air Spike Inlet at Mach 10," AIAA Paper 96-0721, Jan. 1996.

[16]Minucci, M. A. S., Bracken, R. M., Myrabo, L. N., Nagamatsu, H. T., and Shanahan, K. J., "Experimental Investigation of an Electric Arc Simulated Air Spike in Hypersonic Flow," AIAA Paper 00-0715, Jan. 2000.

[17]El-Khabiry, S., and Colver, G. M., "Drag Reduction by DC Corona Discharge Along an Electrically Conductive Flat Plate for Small Reynolds Number Flow," *Physics of Fluids*, Vol. 9, No. 3, 1997, pp. 587–599.

[18]Jagadeesh, G., Srinivasa Rao, B. R., Nagashetty, K., Reddy, N. M., and Reddy, K. P. J., "Electrical Discharge Technique for Three-Dimensional Flow Field Visualization in Hypersonic Shock Tunnel," *Journal of Flow Visualization and Image Processing*, Vol. 4, 1997, pp. 51–57.

[19]Reddy, N. M., "Aerodynamic Force Measurements in the Hypersonic Shock Tunnel," *Proceedings of 14th International Symposium on Shock-Tubes and Waves*, edited by D. A. Archer and B. E. Mitton, Sydney Shock Tube Symposium Publishers, Sydney, Australia, 1983, pp. 358–362.

[20]Srulijes, J., Gnemmi, P., Runne, K., and Seiler, F., "High Pressure Shock Tunnel Experiments and CFD Calculations on Spike-Tipped Blunt Bodies," AIAA Paper 2002-2918, June 2002.

[21]Truitt, R. W., *Hypersonic Aerodynamics*, Ronald, New York, 1959.

[22]"Yearly Review of Aerospace Sciences: Thermophysics," *Aerospace America*, Dec. 2001, pp. 20, 21.

[23]Garanin, A. F., and Glagolev, A. I., "Pressure Variation on the Face Section of the Body of Revolution with a Spike with Variation of Its Length, Geometry and Injection of an Inert Gas from the Spike," *Proceedings of 10th International Conference on the Methods of Aerophysical Research*, Siberian Branch, Russian Academy of Sciences, Novosibirsk, Russia, 2000.

[24]Jagadeesh, G., Reddy, N. M., Nagashetty, K., and Reddy, K. P. J., "Forebody Convective Heat Transfer Measurements over Large-Angle Blunt Cones," *Journal of Spacecraft and Rockets*, Vol. 37, No. 1, 2000, pp. 137–139; also AIAA Paper 98-2601, June 1998.

[25]Reding, J. P., Guenther, R. A., and Jecmen, D. M., "Scale Effects on Fluctuating Pressures in Spike-Induced Flow Separation," *Journal of Spacecraft and Rockets*, Vol. 17, 1980, pp. 112–118.

[26]Calarese, W., and Hankey, W. L., "Modes of Shock-Wave Oscillations on Spike-Tipped Bodies," *AIAA Journal*, Vol. 23, No. 2, 1985, pp. 185–192.

[27]Srinivasa, P., "Experimental Investigations of Hypersonic Flow over a Bulbous Heat Shield at Mach number 6," Ph.D. Dissertation, Dept. of Aerospace Engineering, Indian Inst. of Science, Bangalore, India, Sept. 1991.

[28]Jagadeesh, G., Dhinagaran, R., Haridoss, K., and Reddy, K. P. J., "Convective Heat Transfer Computations over Large Angle Blunt Cones Using CFX TASCflow," AEA Technology, CFX Users' (Intl.) Meeting, Friedrichshafen, Germany, 1999.

M. Sichel
Associate Editor